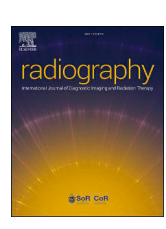


Contents lists available at ScienceDirect

Radiography

journal homepage: www.elsevier.com/locate/radi



Impact of pre-reconstruction filtering with butterworth filter on ¹¹¹In-pentetreotide SPECT image quality and quantitative accuracy: A phantom study



D. Hasegawa ^{1,2}, T. Iguchi ^{3,*}, M. Nakashima ⁴, K. Yoshitomi ⁴, M. Miyai ^{1,5}, K. Kojima ⁶, T. Asahara ³

- ¹ Department of Radiological Technology, Graduate School of Health Sciences, Okayama University, 2-5-1 Shikata-Cho, Kita-Ku, Okayama-Shi, Okayama, 700-8558, Japan
- ² Department of Radiological Technology, Faculty of Health Science, Kobe Tokiwa University, 2-6-2 Otani-cho, Nagata-ku, Kobe, Hyogo 653-0838, Japan ³ Department of Radiological Technology, Faculty of Health Sciences, Okayama University, 2-5-1 Shikata-Cho, Kita-Ku, Okayama-Shi, Okayama, 700-8558, Japan
- 4 Department of Radiological Technology, Okayama University Hospital, 2-5-1 Shikata-Cho, Kita-Ku, Okayama-Shi, Okayama, 700-8558, Japan
- ⁵ Department of Radiology, Kawasaki Medical School General Medical Center, 2-6-1 Nakasange, Kita-Ku, Okayama-shi, Okayama, 700-8505, Japan
- ⁶ Department of Radiology, Okayama University Hospital, 2-5-1 Shikata-Cho, Kita-Ku, Okayama-Shi, Okayama, 700-8558, Japan

ARTICLE INFO

Article history: Received 5 May 2025 Received in revised form 22 July 2025 Accepted 28 July 2025 Available online xxx

Keywords: SPECT Butterworth filter Gaussian filter ¹¹¹In-pentetreotide Quantification

ABSTRACT

Introduction: This study evaluates the image quality and quantitative accuracy of SPECT images with pre- and post-reconstruction smoothing filters in somatostatin receptor scintigraphy using phantom data.

Methods: We evaluated the spatial resolution, the contrast-to-noise ratio (CNR), and the quantitative accuracy using a NEMA IEC body phantom filled with a ¹¹¹In solution. SPECT images were obtained with a Siemens Symbia T16 SPECT/CT system. Quantitative accuracy refers to the ability to accurately estimate the radioactive concentration of ¹¹¹In in the phantom from the image. SPECT reconstructions were performed using three methods: post-reconstruction Gaussian filtering (post-G), pre-reconstruction Gaussian filtering (pre-G), and pre-reconstruction Butterworth filtering (pre-B). To verify each filtering method, the cut-off frequency of the Butterworth filter and the full width at half maximum (FWHM) of the Gaussian filter were each changed to eight different settings.

Results: FWHMs were 21.2, 19.8, and 18.0 mm for post-G, pre-G, and pre-B. CNRs (37-mm sphere) were 47.2, 63.8, and 69.5. Pre-B showed a 12.0 % error rate at 0.40 cycles/cm, while post-G and pre-G showed 20.2 % and 22.0 % at 7.2-mm FWHM. Pre-B outperformed other methods for resolution, CNR, and quantitative accuracy.

Conclusion: For ¹¹¹In-pentetreotide SPECT images, image reconstruction with a Butterworth filter applied to the projection image before reconstruction was found to be superior to reconstruction with a Gaussian filter in terms of image quality and quantitative accuracy.

This method can be easily implemented in routine clinical SPECT imaging workflows and has the potential to improve diagnostic confidence.

Implications for practice: The proposed method with a pre-reconstruction Butterworth filter has great potential to improve the image quality and quantitative accuracy of ¹¹¹In-SPECT images.

© 2025 The Author(s). Published by Elsevier Ltd on behalf of The College of Radiographers. This is an open access article under the CC BY license (http://creativecommons.org/licenses/by/4.0/).

Introduction

Somatostatin receptors are expressed in various cells of the central nervous system, including the pituitary, gastrointestinal tract (pancreas, gastrointestinal tract) and neuroendocrine cells. These receptors are also expressed in tumor cells such as pituitary adenomas and gastrointestinal hormone-secreting tumors.¹

E-mail address: iguchi@s.okayama-u.ac.jp (T. Iguchi).

^{*} Corresponding author.

Somatostatin receptor scintigraphy (SRS) is used to detect neuro-endocrine tumors that express somatostatin receptor (SSTR) 2, 3 and 5. Accurate detection is clinically important because it strongly influences treatment strategies.^{2–4} Although the Society of Nuclear Medicine and Molecular Imaging (SNMMI) and the European Association of Nuclear Medicine (EANM) guidelines have suggested the use of SSTR positron emission tomography (PET) to select patients for peptide receptor radionuclide therapy (PRRT), PET agents such as ⁶⁸Ga-DOTATATE have not yet received pharmaceutical approval in Japan.^{5–7} Therefore, improving the detectability of neuroendocrine tumors using ¹¹¹In-pentetreotide SRS remains an important clinical challenge.

Single photon emission computed tomography (SPECT), a three-dimensional imaging technique, is used in SRS.^{8,9} Projection data obtained from SPECT acquisition are typically reconstructed using iterative methods. Smoothing filters, such as Gaussian filters, are commonly applied after reconstruction to reduce image noise. 10-12 However, post-reconstruction Gaussian filtering may degrade spatial resolution and underestimate pixel values, making it difficult to detect small lesions. 13-15 Therefore, filtering methods that reduce image noise while preserving the spatial resolution of the image are important for the detection of small lesions. There have been many previous studies on improving the image quality by filtering. 16-19 Ito et al. 20 reported a nonlinear diffusion (NLD) method that reduces noise while preserving spatial resolution, but its implementation on commercial clinical devices remains challenging. Therefore, we focused on smoothing filtering methods that are available in commercial clinical devices. Although the SIEMENS SPECT system uses a Gaussian filter as a postreconstruction smoothing filter in the iterative reconstruction, we speculated that image quality could be improved by applying filters to the projection data before image reconstruction. The reason for the standard use of post-reconstruction filtering is not entirely clear, but it is presumed to help reduce Gibbs artifacts, which are a common issue in reconstruction methods that incorporate spatial resolution correction.²¹ The study focusing on such filtering procedures has been reported in simulations, 16 but there are no reports using actual clinical devices. In addition, statistical noise is an issue in SRS because the standard dose of 111 In-pentetreotide is 111 MBq, which is lower than that of ^{99m}Tc. Therefore, it is worthwhile to verify an appropriate smoothing filter method for ¹¹¹In-pentetreotide SPECT images. The aim of this study is to evaluate the image quality and quantitative accuracy of 111 Inpentetreotide SPECT images generated using pre- and postreconstruction smoothing filters with phantom data.

Methods

SPECT acquisition protocol

All data were acquired with a dual-head SPECT/CT system (Symbia T16, Siemens Healthcare, Erlangen, Germany) equipped with a medium-energy low-penetration (MELP) collimator, which had a sensitivity of 8.4 cpm/kBq at gallium-67 (67 Ga) with a 20 % window and a system resolution of 12.5 mm (Full Width at Half Maximum (FWHM) at 10 cm distance). The energy windows for SPECT imaging were 172 keV \pm 10 % and 247 keV \pm 10 % for the main window. All projection data were acquired in step-and-shoot mode for 15 min (60 steps, 30 s/step, 128 \times 128 matrix, magnification 1.0, 4.8 mm/pixel size). The CT imaging conditions were as follows: tube voltage of 130 kV, tube current of 60 mA with CARE Dose $4D^{\rm TM}$, rotation speed of 0.5 s, and slice thickness of 1.5 mm. SPECT acquisition was performed once.

SPECT reconstruction and filtering methods

All images were reconstructed using the Flash3D™ algorithm, integrating attenuation correction according to an attenuation map derived from the CT data. The number of subsets and iterations was set to 10 and 10, respectively, based on the clinical condition. Three different filtering methods were compared (Fig. 1). The conventional method (post-G) reconstructed the SPECT projection data by iterative approximation, and then performed smoothing with a Gaussian filter as a 3D postreconstruction filter. Our proposed methods are to smooth the SPECT projection data with a Gaussian filter (pre-G) and Butterworth filter (pre-B) as 2D pre-reconstruction filters, respectively, and then perform iterative reconstruction using the filtered data. The 2D pre-reconstruction filtering was applied independently on each projection. The cutoff frequency of the Butterworth filter was set to 0.30, 0.35, 0.40, 0.45, 0.50, 0.55, 0.60, and 0.65 (cycles/cm), and the order was set to 8. The FWHM of the Gaussian filter was set to 7.2, 8.4, 9.6, 10.8, 12.0, 13.2, 14.4, and 15.6 (mm). The filter equations used in this study are shown below:

Gaussian filter:
$$F(x,y) = \frac{1}{2\pi\sigma^2} exp\left(-\frac{x^2+y^2}{2\sigma^2}\right)$$
 (1)

Butterworth filter:
$$B(f) = \frac{1}{1 + (f/f_c)^{2n}}$$
 (2)

where, σ is the standard deviation, f_c is the cutoff frequency, n is the order. The FWHM of the Gaussian filter is approximately 12 mm in clinical practice, so the FWHM range was set to fully cover that range. The Butterworth filter parameters were chosen to visually approximate the Gaussian-filtered images. The images with the Butterworth filter as the post-reconstruction filter were not considered in this study because moiré-type artifacts appeared in the reconstructed images.

Phantom design

A NEMA IEC body phantom (Data Spectrum, NC, USA) was used to simulate the upper abdomen. Spheres of the phantom (size: 10-, 13-, 17-, 22-, 28-, and 37-mm diameter) were filled with an ¹¹¹In solution (10.8 kBq/mL), and activity was added to the background compartment to achieve a sphere-to-background ratio of 8:1. This ratio was chosen because it approximates the clinical accumulation observed 24 h after administration in tumors compared to the liver.^{22,23} The cross-calibration factor (CCF) to calculate the radio-activity concentration (Bq/mL) was measured using a cylindrical phantom (diameter 20 cm, volume 6840 mL), which was filled with an ¹¹¹In solution (3.47 kBq/mL). The CCF was calculated as follows:

$$CCF\left(\frac{Bq/mL}{SPECT\ counts/pixel}\right) = \frac{A}{M_{count}}$$
(3)

where A is the decay-corrected activity (Bq/mL) at the start time of the SPECT acquisition, and M_{count} is the mean counts in the region of interest (ROI) drawn on the SPECT transverse image of the cylindrical phantom.²⁴

Image assessment

Spatial resolution

The profile curves were set to a 28-mm diameter hot sphere in both the horizontal and vertical directions on the axial SPECT image using the Daemon Research Image Processor (DRIP; PDR Pharma Co. Ltd, Tokyo, Japan) (Fig. 2). The spatial resolution of

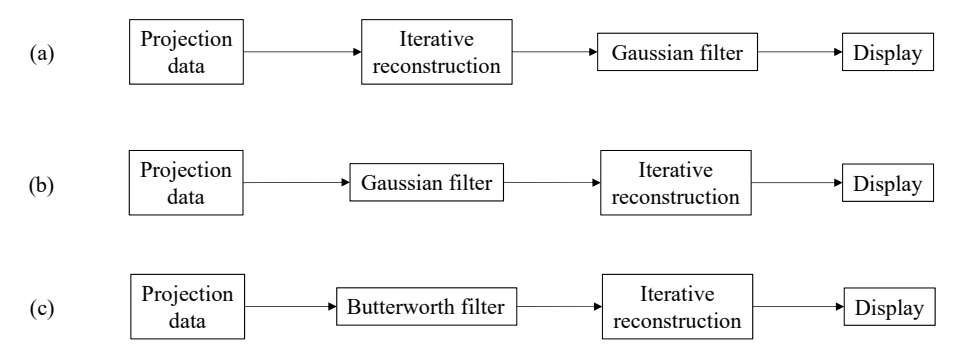


Figure 1. Three different reconstruction and filtering methods. (a) Post-reconstruction Gaussian filtering (post-G), (b) Pre-reconstruction Gaussian filtering (pre-G), and (c) Pre-reconstruction Butterworth filtering (pre-B).

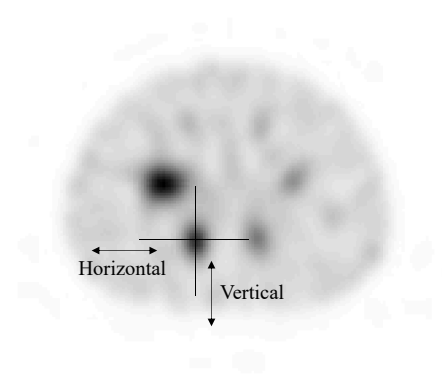


Figure 2. Profile curve setting at 28-mm hot sphere in the horizontal and vertical directions in the axial SPECT image.

each filtering method was evaluated by the average horizontal and vertical FWHM values calculated from each profile curve.

Contrast to noise ratio

The volumes of interest (VOIs) were placed on the 17-, 22-, 28- and 37-mm diameter hot spheres in the SPECT transverse image of the NEMA IEC body phantom using the DRIP (Fig. 3(a)). ²² The VOIs were drawn as spherical regions along the contours of each hot sphere on the CT images and then pasted onto the SPECT images. To evaluate the signal value and noise in the background region, 12 ROIs with a diameter of 37 mm were placed around the periphery of the hot sphere in the SPECT transverse image (Fig. 3(b)). The contrast-to-noise ratio (CNR) was calculated from each SPECT reconstructed image using different filtering methods according to the following formula:

$$CNR = (C_T - C_{BG}) / SD_{BG} \tag{4}$$

where, C_T is the mean counts of the 17-, 22-, 28-, and 37-mm diameter spherical VOIs, C_{BG} is the mean count of the background ROIs which is calculated from 12 circular ROIs of 37 mm in diameter on the phantom background and SD_{BG} is the standard deviation of the background ROIs. Partial volume correction (PVC) was not applied in this study because PVC is not routinely performed in clinical SPECT imaging workflows, and we aimed to evaluate filter performance under standard reconstruction conditions.

Accuracy of quantification

We evaluated the quantitative accuracy of each reconstructed image by three filtering methods using the error rate between the

measured values of the radioactivity concentration in 17-, 22-, 28-, and 37-mm diameter hot spheres and the true values of the radioactivity concentration in the hot spheres. The radioactivity concentrations were calculated as:

Radioactivity concentration
$$(Bq / mL) = M_{count} \times CCF$$
 (5)

The CCF used the values calculated for each filter parameter. The error rate was calculated as:

Error rate (%) =
$$(measured\ value - true\ value)/true\ value \times 100$$
(6)

Statistical analysis

Statistical comparisons of FWHM, CNR, and error rates among the different filtering methods were performed using the Steel–Dwass test. Analyses were conducted with Easy R (Saitama Medical Center, Jichi Medical University, Saitama, Japan), version 1.52, and R (The R Foundation for Statistical Computing, Vienna, Austria), version 4.0.2. A p-value of <0.05 was considered statistically significant.

Results

Spatial resolution

The SPECT reconstruction images and the FWHM results for each filtering method are shown in Figs. 4 and 5, respectively. For each filtering method, the FWHM increased with increasing smoothing strength. When the filtering method was pre-B, the FWHM value was the lowest compared to the other methods, at 18.0 mm when the cut-off frequency was 0.65 cycles/cm (Fig. 5(c)). Statistical analysis also revealed a significant difference in FWHM between pre-B and post-G (p < 0.05). When comparing the post-G and pre-G methods, the lowest FWHM values were 21.2 mm and 19.8 mm, respectively, with the pre-G method showing a lower value (Fig. 5(a and b)). In addition, when the cut-off frequency was above 0.50 cycles/cm in the pre-B method, the change in FWHM was small, and when the cut-off frequency changed from 0.50 to 0.65 cycles/cm, the change in FWHM was only 0.8 mm, whereas in the post-G and pre-G methods, the FWHM changed linearly with the change in smoothing strength.

Contrast to noise ratio

The mean value for each hot sphere and the mean and standard deviation for the background region for each filtering method are shown in Table 1, and the CNR results are indicated in Fig. 6. For each filtering method, the CNR increased as the smoothing

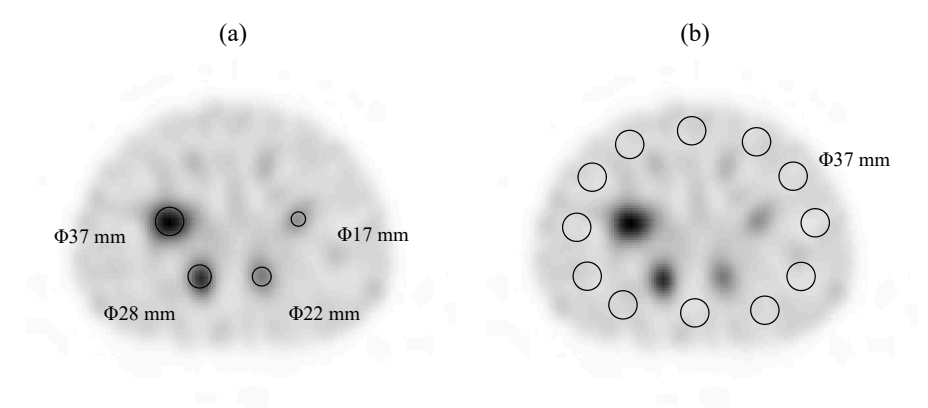


Figure 3. SPECT transverse images of the NEMA IEC Body phantom. (a) Region of interest setting for calculating contrast to noise ratio. (b) Volume of interest setting for calculating contrast to noise ratio and accuracy of quantification.

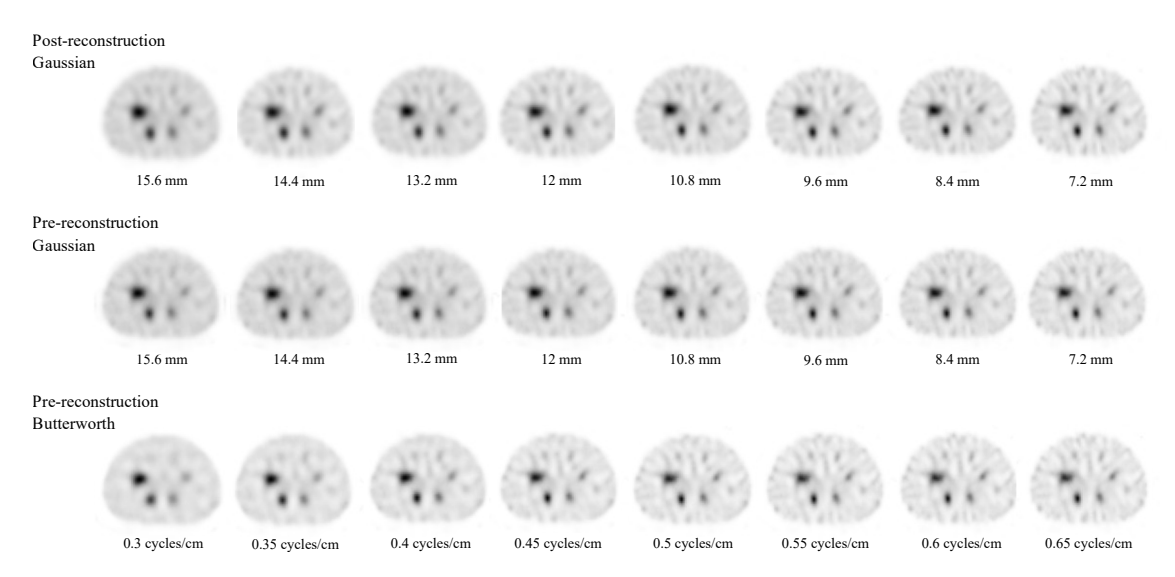


Figure 4. SPECT transverse images of the NEMA IEC Body phantom with different filtering methods. The pre-reconstruction Butterworth method appears to have good contrast because it appears to have relatively low background counts compared to the other filtering methods.

intensity increased; for the 37 mm sphere, the pre-B method had a CNR of 69.5 at 0.30 cycles/cm, the highest value compared to the other methods (Fig. 6(c)). This was also observed for the other sphere sizes, with the pre-B method having the highest CNR, however, statistical analysis showed no significant differences in CNR between each filtering method. The pre-B method had a larger standard deviation in the background region than the other methods, but the hot sphere measurements tended to be higher (Table 1). When comparing the post-G and pre-G methods, the post-G method had a higher CNR when the FWHM of the Gaussian filter was 7.2 mm, but when the FWHM was 8.4 mm or higher, the pre-G method had a higher CNR than the post-G method (Fig. 6(a and b)).

Accuracy of quantification

The error rate between the true and measured values for each hot sphere is shown in Fig. 7. When the sphere diameter was 17 mm, the error rate was large for all filter methods, and the error rates for post-G, pre-G, and pre-B were 54.7 %, 62.2 %, and 51.5 %, respectively, with the pre-B method having the lowest error rate. When the sphere diameter was 37 mm, the error rates for post-G,

pre-G, and pre-B were 20.2 %, 22.0 %, and 12.0 %, respectively, and the quantitative accuracy of pre-B was about 10 % better than the other filter methods. For other sphere sizes, the pre-B method also showed the lowest error rate and statistical analysis showed significant differences in 22 mm, 28 mm, and 37 mm sphere size compared to other filtering methods (p < 0.05). When the post-G and pre-G methods were compared, the post-G method showed an error rate that was approximately 5 % lower. For the pre-G method, the error rate increased strongly, especially with increasing FWHM of the Gaussian filter.

Summary of key performance metrics

To provide an overview of the results, Table 2 summarizes the key performance metrics (FWHM, CNR, and error rate) across the three filtering methods. The values in this table represent the mean \pm standard deviation for the 28-mm hot sphere, which was selected as a representative size for comparison. Statistically significant differences were observed for FWHM and error rate between pre-B and post-G (p < 0.05 and p < 0.01, respectively), while no significant differences were observed in CNR (n.s., Steel–Dwass test).

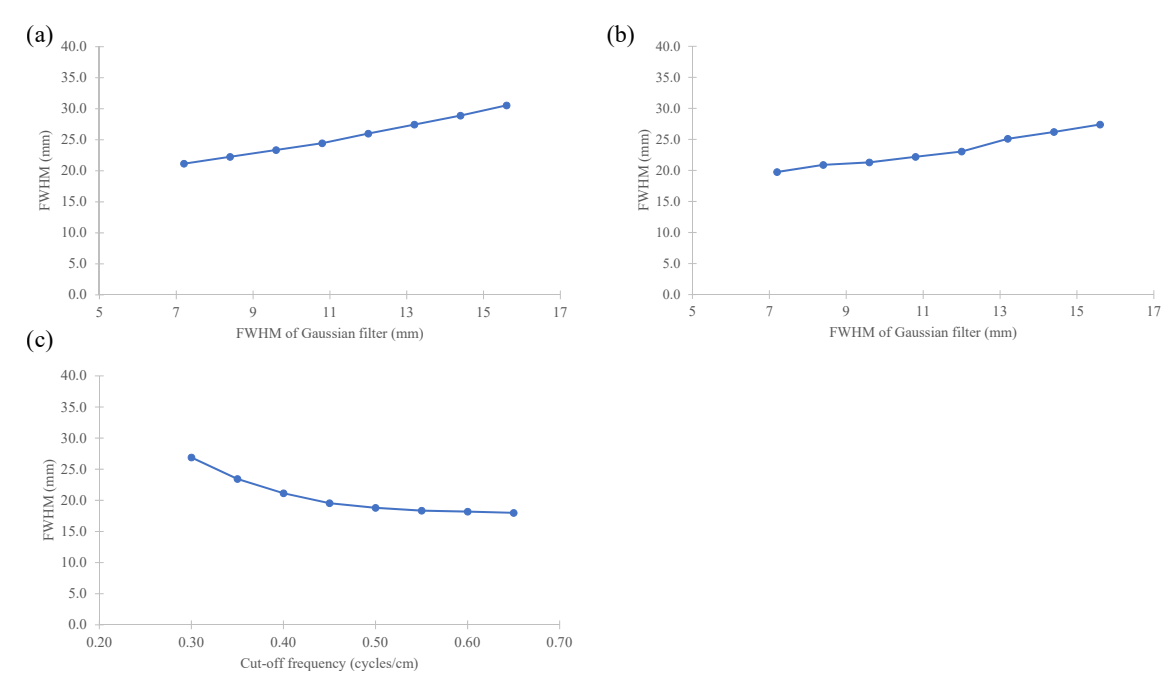


Figure 5. FWHM as a function of filter parameters in each filtering method: (a) Post-reconstruction Gaussian filtering (FWHM = 7.2-15.6 mm), (b) Pre-reconstruction Gaussian filtering (FWHM = 7.2-15.6 mm), and (c) Pre-reconstruction Butterworth filtering (cut-off frequency = 0.30-0.65 cycles/cm). Statistically significant differences in FWHM were observed between pre-B and post-G (p < 0.05). FWHM, full width at half maximum.

Table 1
The mean value for each hot sphere and the mean and standard deviation for the background region for each filtering method: (a) post-reconstruction Gaussian filter, (b) pre-reconstruction Gaussian filter, and (c) pre-reconstruction Butterworth filter.

(a)						
Filter parameter	Sphere diameter				Background	
FWHM of Gaussian filter (mm)	17 mm	22 mm	28 mm	37 mm	mean value	SD
7.2	150.4	181.8	222.9	263.4	48.3	6.1
8.4	147.3	178.3	219.3	260.3	48.1	5.8
9.6	144.4	174.3	215.1	257.0	48.0	5.5
10.8	141.1	170.8	210.9	253.2	47.8	5.2
12.0	137.4	166.8	206.0	249.3	47.6	4.9
13.2	134.0	162.8	201.3	245.0	47.5	4.6
14.4	130.8	158.9	196.1	240.5	47.3	4.3
15.6	127.3	155.0	191.3	239.1	47.1	4.1
(b)						
Filter parameter	Sphere diameter				Background	
FWHM of Gaussian filter (mm)	17 mm	22 mm	28 mm	37 mm	Mean value	SD
7.2	125.3	163.2	204.3	258.6	48.2	5.7
8.4	136.4	169.8	209.8	257.5	48.4	5.2
9.6	132.0	166.0	203.6	252.9	48.4	4.4
10.8	125.2	161.6	196.0	245.4	47.8	4.0
12.0	121.3	155.8	189.4	241.1	47.8	3.7
13.2	115.2	149.3	180.4	233.7	47.9	3.3
14.4	109.6	142.5	173.8	226.5	47.8	3.0
15.6	104.7	136.2	167.5	220.1	47.9	2.7
(c)						
Filter parameter	Sphere diameter				Background	
Cut-off frequency (cycle/cm)	17 mm	22 mm	28 mm	37 mm	Mean value	SD
0.30	121.3	160.3	208.3	283.5	47.8	3.4
0.35	129.2	174.7	225.8	290.3	48.5	4.1
0.40	141.8	186.5	234.9	291.0	48.7	4.7
0.45	149.3	189.8	237.5	288.1	48.8	5.4
0.50	154.3	190.7	236.6	284.3	49.0	5.9
0.55	156.6	191.7	234.7	279.1	48.5	6.3
0.60	159.8	192.3	232.4	277.3	48.8	6.5
0.65	160.3	193.8	234.3	275.5	48.7	6.9

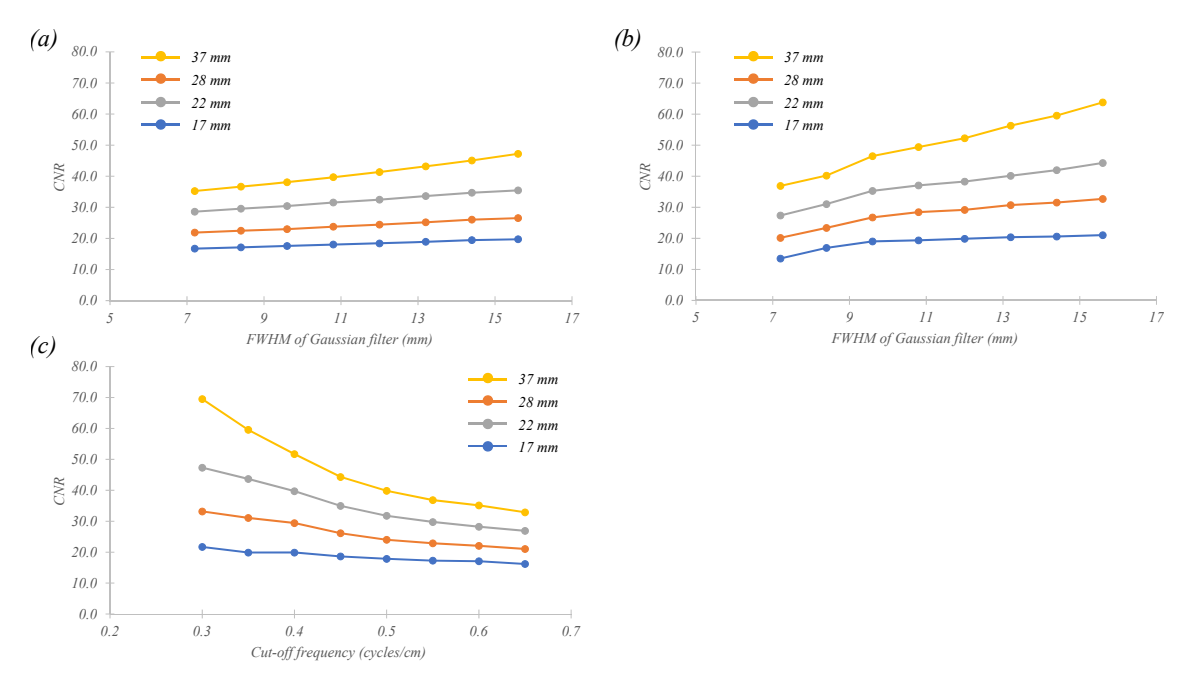


Figure 6. CNR as a function of filter parameters in each filtering method: (a) post-reconstruction Gaussian filter (FWHM = 7.2–15.6 mm), (b) pre-reconstruction Gaussian filter (FWHM = 7.2–15.6 mm), and (c) pre-reconstruction Butterworth filter (cut-off frequency = 0.30–0.65 cycles/cm). No statistically significant differences in CNR were observed among the filtering methods. CNR, contrast to noise ratio.

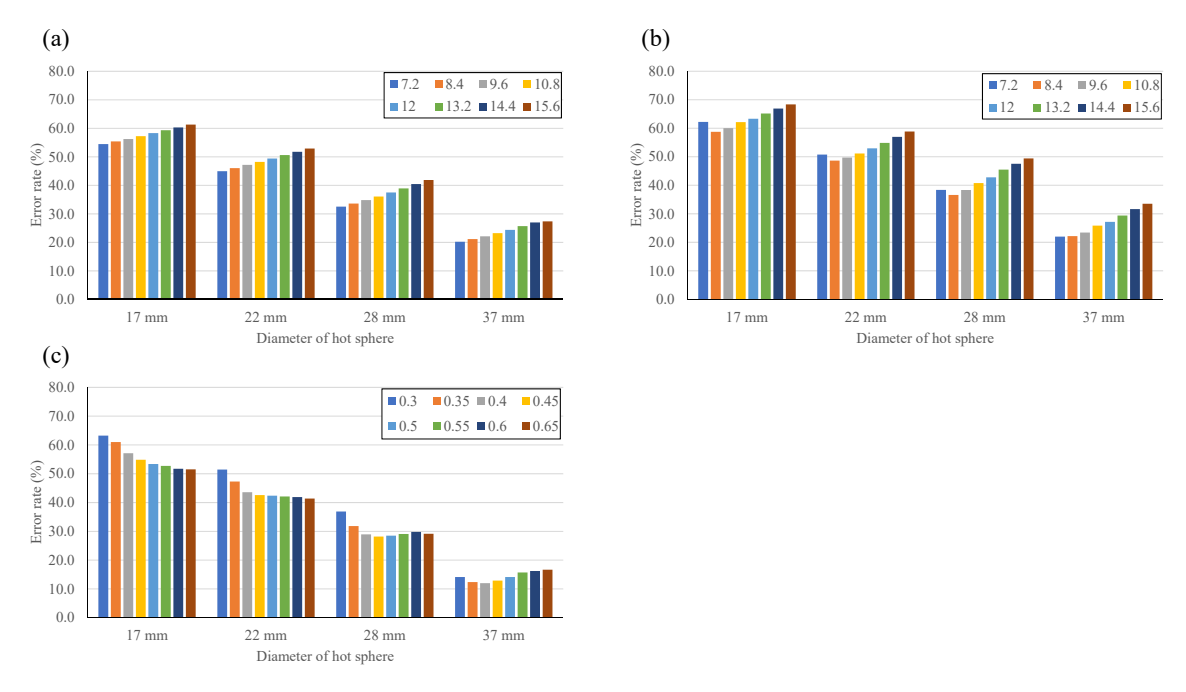


Figure 7. Error rate between the true and measured values at each hot sphere when the filter parameters were changed: (a) post-reconstruction Gaussian filter (FWHM = 7.2–15.6 mm), (b) pre-reconstruction Gaussian filter (FWHM = 7.2–15.6 mm), and (c) pre-reconstruction Butterworth filter (cut-off frequency = 0.30–0.65 cycles/cm). Statistically significant differences were observed as follows: for the 37-mm and 28-mm spheres, p < 0.01 between post-G vs pre-B and pre-G vs pre-B; for the 22-mm sphere, p < 0.05 for post-G vs pre-B and p < 0.01 for pre-G vs pre-B; and for the 17-mm sphere, p < 0.05 for post-G vs pre-G and pre-G vs pre-B.

Table 2 Summary of key performance metrics (mean \pm SD) for the 28-mm sphere across the three filtering methods. P-values were calculated using the Steel–Dwass test for multiple comparisons. n.s., not significant.

Metric	Post-G	Pre-G	Pre-B	p-value
FWHM (mm)	25.5 ± 3.1	23.2 ± 2.6	20.6 ± 3.0	Post-G vs Pre-B: <i>p</i> < 0.05
CNR	32.1 ± 2.2	36.9 ± 5.0	35.3 ± 6.7	n.s.
Error rate (%)	37.0 ± 3.1	42.4 ± 4.4	30.3 ± 2.7	Post-G vs Pre-B: $p < 0.01$;
				Pre-C vs Pre-B: $n < 0.01$

Discussion

In this study, we evaluated the effect of smoothing filter type and method on image quality and quantitative accuracy for SRS SPECT/CT imaging. When we evaluated the spatial resolution based on the FWHM of the profile curve, the pre-B method had the lowest FWHM, which is similar to the results of a previous study that investigated the filter effect before and after reconstruction in a simulation study. Since the Butterworth filter performs noise

rejection by order and cutoff frequency, it can remove noisy high frequency components while preserving low frequency components. The Gaussian filter performs smoothing uniformly regardless of the frequency band, so the low frequency component, the central component of the image, is removed more than necessary. These principles suggest that the FWHM was lower in pre-B than in pre-G and post-G. Previous studies have shown comparable FWHM results for pre-G and post-G¹⁶, but in this study, pre-G showed a slightly lower FWHM than post-G, which may be due to differences in the resolution recovery correction method in the image reconstruction method used in this study. ²⁶

The CNR results showed that the pre-B method showed the highest CNR at 0.30 cycles/cm for all sphere sizes and showed higher values than the pre-G and post-G methods. From these results, it is inferred that the pre-B method can obtain high visibility of spheres of varying sizes in the phantom study, suggesting potential applicability to the detection of neuroendocrine tumors. Focusing on the measurements of the region of interest, the values and standard deviations of the background region were higher in pre-B than in post-G and pre-G, but the measurements of each sphere were also approximately 10 % higher in post-G and pre-G, which likely resulted in a higher CNR (Table 1). This is thought to be because, as mentioned above, the Butterworth filter only removes the high frequency components of the signal components, making it easier to preserve the signal values. When comparing pre-G and post-G, the CNR was higher in pre-G. Although the measured values were higher in post-G, the standard deviation of the background region was lower in pre-G. resulting in a higher CNR in pre-G (Table 1). Wen et al.²⁷ reported contrast reduction by post-filtering with a Gaussian filter after image reconstruction. Furthermore, this CNR result is similar to that of a study comparing pre-G and post-G in ¹²³I-ioflupane SPECT images, demonstrating the usefulness of the prereconstruction filter.²⁸ It is also possible that the smoothing before reconstruction may have resulted in a higher CNR, since some reports indicate that a higher count per projection in iterative reconstruction results in better uniformity.²⁹ However, since the CNR of pre-G and pre-B varies more greatly depending on the filter parameters than that of post-G, care must be taken to set appropriate filter parameters.

In the evaluation of quantitative accuracy, pre-B results showed the lowest error rate compared to post-G and pre-G. Compared in the 37 mm sphere, pre-B showed an error rate of 12.0 % at 0.40 cycles/cm, while post-G showed 20.2 % at a FWHM of 7.2 mm and pre-G showed 22.0 % at a FWHM of 7.2 mm, pre-B had a quantitative accuracy approximately 10 % higher than the other methods. This may be because, as previously mentioned, the Butterworth filter can remove high-frequency components, which are noise. while retaining low-frequency components, thus having less effect on pixel values. 10 The results of using the Gaussian filter, which resulted in lower quantitative accuracy, were similar to many previous studies. 14,15 In addition, even with the 37 mm sphere, there was a quantitative error of more than 10 % in this study. There are many possible factors that can cause this error, including partial volume effect and CCF.^{22,30} Previous studies have also shown an underestimation of more than 10 % with the 37 mm sphere compared to the 44 mm sphere, ²² so the present results are considered valid. Overall, the pre-B method demonstrated the best performance in terms of spatial resolution, CNR, and quantitative accuracy. However, the Butterworth filter is not without limitations. A trade-off exists between spatial resolution and noise suppression, and careful adjustment of filter parameters, especially cutoff frequency and order, is essential to balance noise reduction and preservation of image detail.³¹

We believe these findings may improve the detectability of neuroendocrine tumors in ¹¹¹In-pentetreotide SPECT imaging and contribute to more accurate dosimetry. It has been also reported that ¹¹¹In-octreotide SPECT/CT images are useful for predicting the therapeutic effect of PRRT with ¹⁷⁷Lu-DOTATATE. ³² Therefore, since the quantitative accuracy of ¹¹¹In-octreotide SPECT/CT images is as important as the image quality, we recommend the pre-B method.

The novelty of this study is that it used a real SPECT/CT machine and a torso phantom to investigate the effect of filtering methods before and after image reconstruction on image quality and quantitative accuracy. We also note that the proposed prereconstruction Butterworth filtering method could be integrated into automated reconstruction pipelines or clinical protocols. The pre-B method can be easily set up by anyone by simply performing Butterworth filtering on the projection data in the SIEMENS Healthineers image reconstruction workflow and setting the Gaussian filter after image reconstruction to 0. We believe that this method has merit in that it can easily improve image quality and quantitative accuracy.

This study has three limitations. First, we did not evaluate the clinical data. It is extremely valuable to use clinical data to verify the ability of each filtering method to detect lesions, but since each patient's data has different statistics, we believe it is necessary to verify it using an appropriate method. Second, only one SPECT/CT device was used in our study, and SPECT images may vary depending on the spatial resolution correction methods and the implementation of the Butterworth filter in different vendor systems.²⁶ Although the proposed pre-reconstruction Butterworth filtering method could theoretically be adapted for other vendor systems, reconstruction algorithms and filter settings differ among manufacturers, which may affect performance. There have been recent reports on the use of a Butterworth filter for postreconstruction processing with a General Electric SPECT/CT system.³³ Therefore, further studies using a variety of commercially available devices are needed to evaluate the broader applicability of this method. Third, the phantom experiment was performed only once because previous studies using the same SPECT/CT system under standardized conditions have demonstrated high reproducibility.³⁴ Moreover, creating phantoms with precisely the same radioactivity concentration is technically challenging and may introduce variability across repeated experiments. Considering these factors and the relatively high cost of ¹¹¹In, multiple acquisitions were not performed. In the future, we plan to validate this method using different radioactivity concentration ratios to further enhance its clinical applicability.

Conclusion

In ¹¹¹In-pentetreotide SPECT imaging, applying a Butterworth filter to the projection data prior to image reconstruction demonstrated improved image quality and quantitative accuracy compared to conventional post-reconstruction Gaussian filtering. This pre-reconstruction filtering approach is practical and easy to implement, as it can be readily integrated into routine clinical image processing workflows without disrupting existing protocols.

Ethics approval and consent to participate

This research did not require Institutional Review Board approval because it was a phantom study that did not use clinical data.

Availability of data

Data required for this study may be made available by the authors upon reasonable request.

Author contributions

Daisuke Hasegawa: Conceptualisation, Methodology, Validation, Formal Analysis, Writing - Original Draft.

Toshihiro Iguchi: Conceptualisation, Supervision, Project Administration, Writing - Review & Editing.

Masahiro Nakashima: Methodology, Validation, Investigation, Resources, Writing - Review & Editing.

Keisuke Yoshitomi: Resources, Data Curation, Writing - Review & Editing.

Masahiro Miyai: Methodology, Writing - Review & Editing. Katsuhide Kojima: Resources, Investigation, Writing - Review & Editing.

Takashi Asahara: Resources, Writing - Review & Editing.

Generative AI use

Not applicable.

Funding

This research received no specific grant from any funding agency in the public, commercial, or not-for-profit sectors.

Conflicts of interest

The authors declare that they have no competing interests.

Acknowledgements

The authors thank to all the staff of Okayama University Hospital for providing the experimental environment, including the SPECT/CT equipment.

References

- 1. Patel YC, Greenwood MT, Panetta R, Demchyshyn L, Niznik H, Srikant CB. The somatostatin receptor family. *Life Sci.* 1995;57:1249–1265.
- Reubi JC, Schär JC, Waser B, Wenger S, Heppeler A, Schmitt JS, et al. Affinity
 profiles for human somatostatin receptor subtypes SST1-SST5 of somatostatin
 radiotracers selected for scintigraphic and radiotherapeutic use. Eur J Nucl
 Med. 2000;27(3):273–282.
- Kwekkeboom D, Krenning EP, Jong M de. Peptide receptor imaging and therapy. J Nucl Med. 2000;41:1704–1713.
- Oberg K. Molecular imaging radiotherapy: theranostics for personalized patient management of neuroendocrine tumors (NETs). *Theranostics*. 2012;2(5): 448–458.
- Hope TA, Auerbach MA, Bodei L, Calais J, Dahlbom M, Dunnwald LK, et al. SNMMI procedure Standard/EANM practice guideline for SSTR PET: imaging neuroendocrine tumors. J Necl Med. 2023;64(2):204–210.
- Hasegawa S, Kobayashi N, Tokuhisa M, Goto A, Takano S, Takada Y, et al. Clinical usefulness of somatostatin receptor scintigraphy in Japanese patients with gastroenteropancreatic neuroendocrine tumors. *Digestion*. 2017;96(1): 13–20
- Deppen SA, Blume J, Bobbey AJ, Shah C, Graham MM, Lee P, et al. ⁶⁸Ga-DOTATATE compared with ¹¹¹In-DTPA-Octreotide and conventional imaging for pulmonary and gastroenteropancreatic nueroendocrine tumors: a systematic review and meta-analysis. *J Nucl Med*. 2016;57:872–878.
- Magnander T, Wikberg E, Svensson J, Gjertsson P, Wängberg B, Båth M, et al. A novel statistical analysis method to improve the detection of hepatic foci of ¹¹¹In-octreotide in SPECT/CT imaging. *EJNMMI Physics*. 2016;3:1.
- Sainz-Esteban A, Olmos R, González-Sagrado M, González ML, Ruiz MA, García-Talavera P, et al. Contribution of 111In-pentetreotide SPECT/CT imaging to conventional somatostatin receptor scintigraphy in the detection of neuro-endocrine tumours. Nucl Med Commun. 2015;36(3):251–259.

- Lyra M, Ploussi A. Filtering in SPECT image reconstruction. Int J Biomed Imag. 2011;2011:693795.
- 11. Sayed IS, Ismail SS. Comparison of low-pass filters for SPECT imaging. Int J Biomed Imag, 2020;2020;9239753.
- Brambilla M, Cannillo B, Dominietto M, Leva L, Secco C, Inglese E. Characterization of ordered-subsets expectation maximization with 3D post-reconstruction gauss filtering and comparison with filtered backprojection in ^{99m}Tc SPECT. Ann Nucl Med. 2005;19(2):75–82.
- Armstrong IS, Hoffmann SA. Activity concentration measurements using a conjugate gradient (siemens xSPECT) reconstruction algorithm in SPECT/CT. Nucl Med Commun. 2016;37(11):1212–1217.
- Tomita Y, Ichikawa Y, Hashizume K, Sakuma H. Effect of gaussian smoothing filter size for CT-Based attenuation correction on quantitative assessment of bone SPECT/CT: a phantom study. J Digit Imag. 2023;36(5):2313–2321.
- Schepers R, Gözlügöl N, Zeimpekis K, Bregenzer CM, Gräni C, Afshar-Oromieh A, et al. The impact of different reconstruction parameters on quantitative ^{99m}Tc-DPD SPECT/CT values in the assessment of cardiac transthyretin amyloidosis. *Int J Cardiovasc Imag.* 2024;40(11):2317–2324.
 Matsutomo N, Tanaka T, Nagaki A, Sasaki M. Validation of noise reduction in
- Matsutomo N, Tanaka T, Nagaki A, Sasaki M. Validation of noise reduction in iterative reconstruction: a simulation phantom study. Nihon Houshasen Gijutsu Gakkai Zasshi. 2014;70(8):773–783.
- Rahimian A, Etehadtavakol M, Moslehi M, Ng EYK. Myocardial perfusion single-photon emission computed tomography (SPECT) image denoising: a comparative study. *Diagnostics*. 2023;13(4):611.
- Perona P, Malik J. Scale-space and edge detection using anisotropic diffusion. IEEE Trans PAMI. 1990;12:629–639.
- Nakashima M, Kangai Y. Evaluation of post-reconstruction filtering in resolution recovery reconstruction for bone SPECT imaging. Nihon Housyasen Gijutsu Gakkai Zasshi. 2020;76(10):1025–1034.
- Ito T, Onoguchi M, Ogata Y, Matsusaka Y, Shibutani T. Evaluation of edgepreserving and noise-reducing effects using nonlinear diffusion method in bone single-photon emission computed tomography. *Nucl Med Commun*. 2019;40(7):693–702.
- 21. Maeda Y, Nagaki A, Komi Y, Abe N, Kashimura S. Evaluation of resolution correction in single photon emission computed tomography reconstruction method using a body phantom: study of three different models. *Nihon Housyasen Gijutsu Gakkai Zasshi*. 2015;71(11):1070–1079.
- 22. Yamashita K, Miyaji N, Motegi Z, Terauchi T, Ito S. Development of a new quantification method using partial volume effect correction for individual energy peaks in ¹¹¹In-pentetreotide SPECT/CT. Asia Ocean J Necl Med Biol. 2022;10(2):126–137.
- 23. Bombardieri E, Ambrosini V, Aktolun C, Baum RP, Bishof-Delaloye A, Vecchio SD, et al. 111In-pentetreotide scintigraphy: procedure guidelines for tumor imaging. *Eur J Nucl Med Mol Imaging*. 2010;37(7):1441–1448.
- Hishikawa M, Matsutomo N, Yamamoto T. Optimization of scatter estimation window setting for quantitative analysis in 111In-pentetreotide single photon emission computed tomography imaging. *Hellenic J Nucl Med.* 2020;23(3): 223–228.
- Kanda Y. Investigation of the freely available easy-to-use software 'EZR' for medical statistics. Bone Marrow Transplant. 2013;48(3):452–458.
- Onishi H, Motomura N, Fujino K, Natsume T, Haramoto Y. Quantitative performance of advanced resolution recovery strategies on SPECT images: evaluation with use of digital phantom models. *Radiol Phys Technol.* 2013;6(1): 42–53.
- 27. Wen L, Eberl S, Wong KP, Feng D, Bai J. Effect of reconstruction and filtering on kinetic parameter estimation bias and reliability for dynamic SPECT: a simulation study. *IEEE Trans Nucl Sci.* 2005;52(1):69–78.
- Larsson A, Mo JS, Sundström T, Riklund K. Gaussian prefiltering of 123I DAT SPECT images when using depth-independent resolution recovery. *Phys Med Biol.* 2007;52(18):N393–N399.
- Hasegawa D, Iguchi T, Takatani M, Tokunaga K, Minoda T, Miyai M. Effect of single-photon emission computed tomography acquisition method and sampling angles on image quality and quantitative accuracy in xSPECTreconstructed images. Nucl Med Commun. 2024;45(11):916–923.
- Matsutomo N, Matsumoto S, Yamamoto T, Sato E. Validation of a calibration method using the cross-calibration factor and system planar sensitivity in quantitative single-photon emission computed tomography imaging. *Radiol Phys Technol*. 2017;10(4):439–445.
- Lewitt RM, Matej S. Overview of methods for image reconstruction from projections in emission computed tomography. *Proc IEEE*. 2003;91(10): 1588–1611.
- Wets C, Apostolova A, Steffen IG, Hofheinz F, Furth C, Kupitz D, et al. Predictive value of asphericity in pretherapeutic [111In]DTPA-Octreotide SPECT/CT for response to peptide receptor radionuclide therapy with [177Lu]DOTATAE. Mol Imag Biol. 2017;19(3):437–445.
- Saib DMA, Azman NZN, Said MA, Aseri MIM, Almarri HM, Ramli RM. Evaluation of butterworth post-filtering effects on contrast and signal noise to ratio values for SPECT images reconstruction. *Radiat Phys Chem.* 2022;192: 109932.
- 34. Okuda K, Hasegawa D, Kamiya T, Ichikawa H, Umeda T, Ohkubo T, et al. Multicenter study of quantitative SPECT: reproducibility of ^{99m}Tc quantitation using a conjugated-gradient minimization reconstruction algorithm. *J Nucl Med Technol.* 2021;49(2):138–142.